Understanding the Activity of Single-Atom Catalysis from Frontier Orbitals

Zhaoming Fu,[1] Bowen Yang,[1] and Ruqian Wu[2,*]
[1]School of Physics, Henan Normal University, Xinxiang, Henan 453007, China
[2]Department of Physics and Astronomy, University of California, Irvine, California 92697-4575, USA

(Received 4 September 2019; revised 16 August 2020; accepted 11 September 2020; published 8 October 2020; corrected 20 October 2020)

The *d*-band center and charge states are often used to analyze the catalytic activity of noble or transition metal surfaces and clusters, but their applicability for single-atom catalysts (SACs) is unsure. This work suggests that the spatial structure and orientation of frontier orbitals which are closest to the Fermi level of SACs play a vital role. Taking adsorption of several molecules and CO oxidization on C_3N-supported single-atom Au as examples, we demonstrate that adsorption and catalytic activities are well correlated with the characteristics of frontier orbitals. This work provides an effective guidance for understanding the performance of single-atom catalysts.

DOI: 10.1103/PhysRevLett.125.156001

Single-atom catalysis is an exciting research subject in recent years, as it has great potential to provide unmatched high reactivity and selectivity for many important reactions and yet much reduced consumption of precious materials [1–8]. Noble metals such as Au are among the most attempted active elements in single-atom catalysts (SACs) for CO oxidation and a few other chemical processes [9–14]. Experimentally, it is puzzling that Au atoms are catalytically active on some substrates [11,14–18] but inactive on others [19–21]. This large swing calls for theoretical explanations so as to identify rational strategies for the optimization of their catalytic properties. The traditional noble metal catalysts are designed with macroscale surfaces and more recently with nanoclusters. Analyses on the *d*-band center and charge state have been rather successful to predict the trend of catalytic activities in different environments. However, the applicability of these approaches for the studies of SACs appears to be questionable. For example, recent studies of the Au SAC brought about an intense debate on which charge states are catalytically more active [22–25]. Therefore, universal mechanisms and simple guiding rules for the design of SACs remain to be explored.

One may ask what the main difference between SACs and traditional metallic catalysts is, so they may follow drastically different rules. One obvious factor is that active metal atoms are sparse and are separated by large spaces in the former, whereas they mutually interact and form broad bands in the latter. As the adsorbates and reactants interact with only one active atom in SACs, the wave function matching between the their lowest unoccupied molecular orbital (LUMO) or the highest occupied molecular orbital (HOMO) and the atomic orbitals closest to the Fermi level of SACs, named the frontier orbitals (FOs) in the following discussions, becomes extremely important. Obviously, reactants and SACs do not hybridize without appropriate orbital matching even if they have orbitals close in energy. Therefore, the wave function characteristics of SAC's FOs should be the foremost issue for the analyses of single-atom catalysis. Indeed, the importance of FOs in zeolite catalysts has been recently brought into attention [26]. It is plausible that FOs' details can be determined using the maximally localized Wannier function (MLWF) method [27] and the crystal field theory nowadays, and, hence, this type of analyses becomes very convenient.

In this work, we take the C_3N-supported Au SACs as examples to investigate the correlation between their FOs and catalytic activities. C_3N is a new graphene-based material with a hexagonal structure [see Fig. 1(a)] and inherits many merits of graphene such as structural flexibility and thermostability. Au/C_3N SACs own noticeable advantages that are suitable for fundamental studies as different coordination modes and charge states,

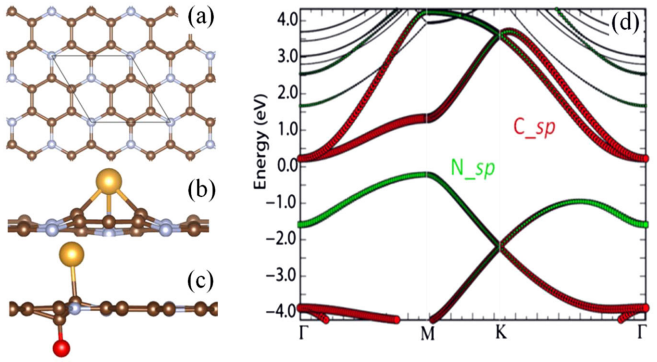

FIG. 1. (a) C_3N primitive cell, in which C and N atoms are shown in brown and gray, respectively. (b) Single Au atom bonded on the C-deficient C_3N. (c) Single Au atom bonded on the O-modified C_3N. (d) Band structure of the pristine C_3N monolayer.

including Au^+, Au^-, and neutral Au (Au^0), can be achieved by modifying the C_3N substrate as depicted in Figs. 1(b) and 1(c). As FOs alter with the change of charge state or geometry, this allows us to separately investigate different factors and correlate FO characteristics with chemical activity and catalytic performance and to establish simple rules for guiding the design of high-performance SACs. Furthermore, the MLWF method has been used for studies of various properties of materials [28–31] but rarely for studies of catalysis. This work, hence, bridges knowledge from different fields.

All computational details are given in Supplemental Material [32], so we may directly discuss results, starting from the structural stability. Unlike zero band-gap graphene, a pristine C_3N monolayer has a band gap of 0.39 eV [see Fig. 1(d)] [49,50], and its work function is also smaller than that of graphene [51,52]. The calculated binding energy of the Au atom on C_3N is 0.93 eV. Although this value is not small compared to Au on other two-dimensional van der Waals substrates such as graphene (0.37 eV), the energy barrier for Au segregation on C_3N is low, only 0.11 eV. Therefore, Au atoms may easily aggregate on pristine C_3N, as also evidenced by *ab initio* molecular dynamics (AIMD) simulations in Fig. S1 [32]. In order to stabilize Au/C_3N SACs, we introduce the C vacancy and O modification (see Fig. S2 and discussions regarding the possibility of making this modification [32]) in the C_3N substrates to anchor single Au atoms [see Figs. 1(b) and 1(c)]. Experimentally, the oxygen modification has been used to enhance the stability of single-atom Au on the substrates of graphitic carbon nitride [32]. Indeed, the binding energies of Au increase to 2.45 and 1.53 eV on these two defected surfaces, respectively. The corresponding energy costs (1.52 and 0.6 eV, respectively) for dragging the Au atom from these defect sites to the smooth areas should be adequate to prevent sparse Au adatoms from escaping. Furthermore, the formation of Au dimers, by moving one Au adatom to the adjacent Au adatom from the defected site, is unfavorable in energy, with a cost of 2.0 and 0.1 eV on the C-deficient or O-modified C_3N, respectively. The AIMD simulations at room temperature also show that the single-atom geometries are sustainable on two defected C_3N within a few picoseconds (see Table S1 and Figs. S1 and S3 [32]). Although the period of simulations is truly short, we may view these results as indicatives of the structural stability of defected Au/C_3N SACs.

Interestingly, the charge state of Au on pristine and O-modified C_3N is negative according to the Bader charge analysis for different coverage [Figs. S4(a) and S4(b) [32]], a status which is considered to be favorable for enhancing the catalytic activity of Au [53–55]. Au adatoms can even become neutral on an O-modified C_3N substrate as the density of oxygen increases [see Fig. S4(c) [32]]. In contrast, the calculated Bader charge of Au becomes positive and has a magnetic moment of 1 u_B on the C-deficient C_3N [see Fig. S4(a) [32]]. Overall, stable single-atom Au^+, Au^-, and Au^0 configurations on C-deficient and O-modified C_3N substrates provide ideal cases for studies of the correlation among chemical activity, charge state, and FO characteristics. To this end, we use molecular adsorbates and CO oxidization reaction as probes in the following discussions.

TABLE I. Adsorption energies (eV) of various gas molecules on negatively and positively charged Au. The values in bracket are O—O bond elongation (Å).

	H_2	O_2	N_2	NH_3
Au^-	0.20	0.64 (0.057)	0.31	0.96
Au^0	0.58	0.76 (0.057)	0 .71	1.43
Au^+	2.11	2.28 (0.178)	0.87	1.44

The optimized adsorption configurations of H_2, O_2, N_2, and NH_3 molecules are shown in Fig. S5 [32]. We especially focus on the O_2 adsorption in the following discussions due to its importance in many chemical processes [56–58]. The calculated adsorption energies in Table I suggest that the Au atom in the positive charge state is more active for gas adsorption than in the neutral or negative charge state. A remarkable rule is that the value of E_{ad} increases with the reduction of the number of electrons on Au. In the brackets of Table I, the elongation of the O—O bond also indicates that Au^+ is active for O_2 dissociation than Au^-, as was also reported for other cases [15,59]. A similar trend was found for H_2 dissociation in our calculations, as E_{ad} increases to 2.11 eV and the H-H distance expands to 2.7 Å on Au^+. However, this appears to contradict with common believes that single Au atoms in the negatively charged state are more activate [22,24,54,55]. Therefore, the correlation between the charge state and chemical activity remains unresolved for Au SACs.

The *d*-band center is often regarded as a key quantity for the activity of noble metal catalysts such as surfaces, films, and nanocluster [60–62]. For single-atom Au in this work, the *d* orbitals of Au are split by the crystal field of the substrate as they form discrete levels as shown in Fig. 2. If we take the averaged energy positions of all *d* orbitals as the "*d*-band center," the corresponding values of Au^- and Au^0 on the O-modified C_3N are −2.72 and −3.28 eV, closer to the Fermi energy than that of Au^+ on the C-deficient C_3N, −3.96 eV. However, the adsorption energies for H_2 and O_2 on Au^- and Au^0 are obviously smaller than those on Au^+, and, hence, the applicability of the *d*-band center is questionable for the present SACs. To understand the reason, it is instructive to compare the electronic structures of *d* orbitals of single-atom Au, Au surface, and Au cluster. Figures S6(a) and S6(b) show the PDOS of five *d* orbitals of the Au(111) surface and Au cluster (Au_{56}) [32]. A remarkable common characteristic for these two cases is the strong hybridization among Au *d* orbitals in a broad energy

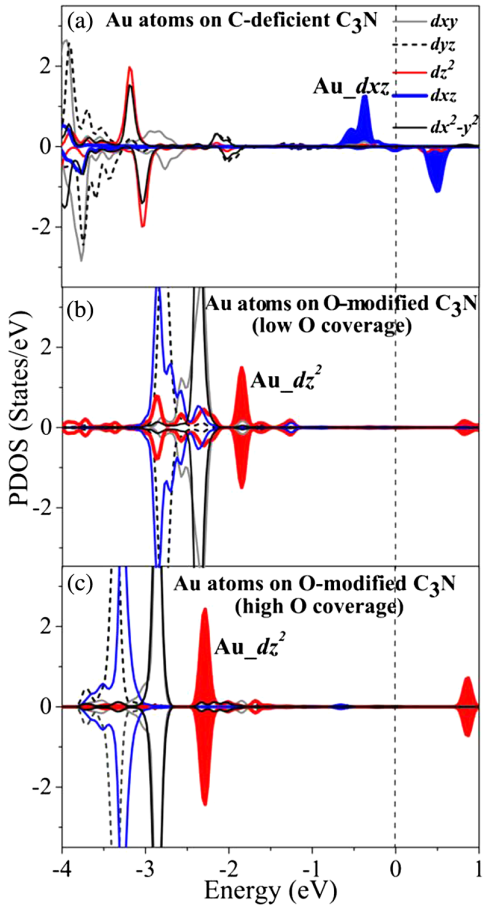

FIG. 2. Projected density of states (PDOS) of Au d orbitals in C-deficient (a) and O-modified C_3N (b),(c). Their frontier orbitals are highlighted. Positive and negative DOS values indicate spin-up and spin-down components, respectively.

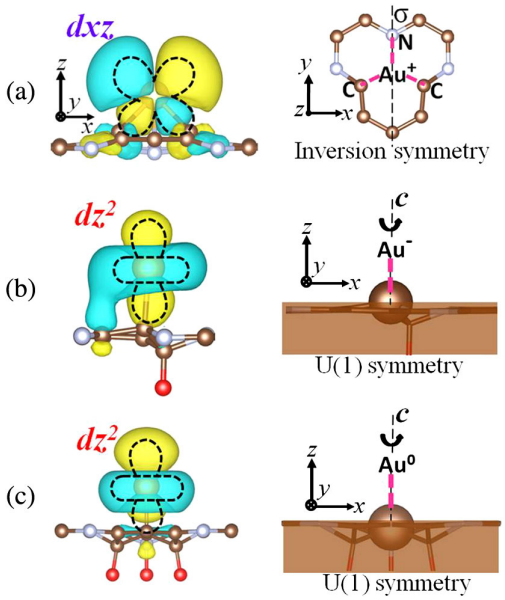

FIG. 3. Calculated Wannier functions of frontier d orbitals of single-atom Au in two different crystal fields, where yellow (+) and light blue (−) represent the sign of the Wannier function. (a)–(c) correspond to defective C_3N and O-modified C_3N with low and high O coverages, respectively.

range, and there is no obvious sequence issue among them. In contrast, the d orbitals of single-atom Au split into discrete levels as shown in Figs. 2(a)–2(c), and their sequence strongly depends on the substrate. For the interaction between two quantum states (e.g., one from Au and the other from absorbates), the overlap between their wave function (or, equivalently, the hopping integral) is as important as their energy separation. Since more than one metal atom on surfaces or clusters interact with adsorbates and all d orbitals participate to some extent, their activity can be reasonably described by an average quantity, i.e., the d-band center. For SACs, adsorbates or reactants mostly interact with one metal atom, and the wave function matching becomes critical. It is also conceivable that FOs are the most important ones due to the small energy separation with the HOMO and LUMO of adsorbates or reactants. We also examined the effect of using a hybrid functional on the description of C_3N. While the band gap agrees better with the experimental value [63], the orbital sequence and Wannier functions are not much different from PBE results (see Figs. S7 and S8 [32]). Therefore, we focus on PBE results in our following discussions.

In principle, the d-level splitting and sequence depend on the crystal fields of the substrates. As shown in Fig. 2, the FO of Au^+ on the C-deficient C_3N is d_{xz}, whereas the FO of both Au^0 and Au^- on the O-modified C_3N is d_{z^2} (Au^0 has a higher PDOS peak and lower energy position). The wave function features of FOs can be better appreciated through Wannier functions. As shown in Fig. 3(a), Au on the C-deficient C_3N interacts with two C and one N atoms, and the crystal field has a mirror symmetry with respect to the y-z plane. Among the five d-orbitals [see Fig. S9(a) [32]], the d_{xz} orbital is the highest in energy. On the O-modified surface, Au takes the top site over a C atom, and the crystal field around Au has a quasi-U(1) symmetry by leaving out the next-nearest neighbor interaction, as shown in Figs. 3(b) and 3(c). The d_{z^2} vertical orbital becomes the highest in energy [see the left side of Figs. 3(b) and 3(c); other Wannier functions are shown in Fig. S9(b) [32]].

To discuss the role of FOs for chemical activities of SACs, we take O_2 adsorption and CO oxidization as examples, as they are involved in many chemical processes. Obviously, O_2 adopts very different adsorption configurations on the C-deficient and O-modified Au/C_3N, as shown in Figs. 4(a) and 4(b). The optimized geometries are independent of the initial structural setting and are driven by the tendency of matching the Au's FOs and the LUMO of O_2 [see Fig. 4(c)]. On the C-deficient Au/C_3N, the FO is d_{xz}, which matches well with the $2\pi^*$ orbital of O_2 in a

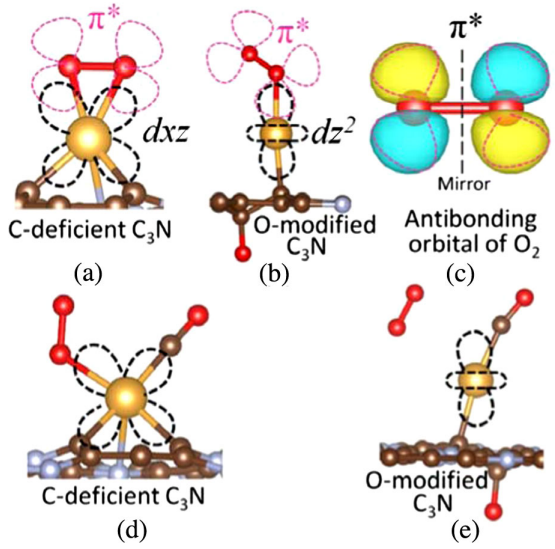

FIG. 4. Different adsorption and coadsorption configurations on single-atom Au with two different frontier orbitals (a),(b) for the adsorption of O_2 and (d),(e) for the coadsorption of CO and O_2. (c) The antibonding orbital of O_2 calculated by MLWF method.

horizontal adsorption geometry depicted in Fig. 4(a). In contrast, only a tilted adsorption geometry allows the formation of one Au—O bond between the $2\pi^*$ orbital of O_2 and the FO (d_{z^2}) of O-modified Au/C_3N, as shown in Fig. 4(b). The level of hybridization between FOs of Au and $2\pi^*$ orbital of O_2 dictates the binding energy in these two cases [see Figs. 4(a)–4(c) and corresponding values in Table I].

For the dissociation of O_2, electron transfer from catalysts to the unoccupied antibonding $2\pi^*$ orbital of O_2 is essential. That is the main reason why negatively charged Au catalysts are often preferred. For Au_n clusters or Au_n substrates, O_2 molecules may easily dissociate at the corner or edge sites or the three-phase boundaries (TPBs) (Fig. S10 [32]) [64,65], where two O atoms bind to separate Au atoms and substrate atoms. This status can be somewhat achieved on the C-deficient Au/C_3N SAC via the two lobes of the d_{xz} FO as shown in Fig. 4(a). As this FO is also close to the Fermi level, Au-O_2 hybridization is strong and the $2\pi^*$ orbital of O_2 extends its tail to below the Fermi level and, hence, receives some electrons, even if Au is in a positively charged state. The partial occupation of the antibonding state certainly activates the dissociation of O_2. In contrast, the d_{z^2} FO leads to the tilted geometry of O_2 on the O-modified Au/C_3N with a weak wave function overlap. Along with the large energy separation between FO and the $2\pi^*$ orbital, this leads to much weaker Au-O_2 hybridization and charge transfer, even if Au has a negative charge state on the O-modified C_3N [see Fig. 4(b)]. Therefore, the ability of hybridizing with the $2\pi^*$ orbital rather than the negative charge state plays the major role in activating O_2 dissociation on these SACs.

CO oxidation on a SAC may follow either the Eley-Rideal (ER) mechanism or the Langmuir-Hinshelwood (LH) mechanism, starting from two different initial states: $O_2^* + CO$ (g) and O_2 (g) + CO^*, respectively. Here, "*" and "g" represent the adsorbed phase and gas phases, respectively. For the ER mechanism, O_2 adsorption and dissociation is the precursor of CO oxidation, and CO directly attaches to one of the O atoms. The transition states for CO oxidation on the two Au/C_3N SACs are searched by using the climbing image–nudged elastic band method (see Fig. S11 [32]). The calculated activity energies are 0.47 eV on the C-deficient Au/C_3N SAC and 0.74 eV on the O-modified Au/C_3N SAC, supporting our argument that the wave function matching is crucial for the catalytic performance of SACs.

For the LH mechanism of CO oxidization, previous studies suggested that the reaction often undergoes a process of coadsorption of CO and O_2 [66]. On the C-deficient Au/C_3N, the optimized geometry in Fig. 4(d) shows a stable coadsorption configuration with O_2 and CO separately attaching to two lobes of the FO. In contrast, CO and O_2 cannot simultaneously form bonds with O-modified Au/C_3N SAC as the d_{z^2} FO only has one outward lobe [see Fig. 4(e)]. Again, these results are independent of the initial structural setting (see Fig. S12 [32]) and are the consequences of having different FOs in the two SACs. The calculated energy barrier of the rate-determining step of CO oxidation on the C-deficient Au/C_3N via the LH mechanism is about 0.32 eV (see Fig. S13 [32]). On the O-modified Au/C_3N, the LH reaction path is blocked, because the intermediate coadsorption of CO and O_2 is absent. Again, these results show that different FOs control the adsorption, coadsorption, and reaction for SACs (see the schematic in Fig. S14 [32]).

In summary, we propose that spatial structures of frontier d orbitals play a vital role for the chemical and catalytic activities of single-atom catalysts. This stems from the requirement of having adequate wave function overlap for SACs to attract adsorbates and reactants, as demonstrated through discussions for adsorptions of small molecules and CO oxidation reaction on the Au/C_3N SACs. The reasoning is general and should be applicable to other SACs. This paves a convenient way for the estimation of catalytic performance of SACs based on the matching between their FOs and LUMOs of reactants, much like the use of the d-band center model for metal surfaces and clusters. Additionally, the present work bridges Wannier function construction from solid state calculations with periodic unit cells and conventional bond analysis in chemical physics. For example, Wannier functions can also provide insightful images for the understanding of "the lone pair-surface bonds" [48] in NH_3 and H_2O adsorptions on different surfaces (see Figs. S15 and S16 [32]).

This work was supported by the National Natural Science Foundation of China (Grant No. U1804130),

Henan Overseas Expertise Introduction Center for Discipline Innovation (Grant No. CXJD2019005) and the High Performance Computing Centre of Henan Normal University. Work at UCI was supported by the National Science Foundation under Grant No. CHE-1905121.

*wur@uci.edu

[1] H. Wei, X. Liu, A. Wang, L. Zhang, B. Qiao, X. Yang, Y. Huang, S. Miao, J. Liu, and T. Zhang, Nat. Commun. **5**, 5634 (2014).
[2] J. Lin, A. Wang, B. Qiao, X. Liu, X. Yang, X. Wang, J. Liang, J. Li, J. Liu, and T. Zhang, J. Am. Chem. Soc. **135**, 15314 (2013).
[3] B. Qiao, A. Wang, X. Yang, L. F. Allard, Z. Jiang, Y. Cui, J. Liu, J. Li, and T. Zhang, Nat. Chem. **3**, 634 (2011).
[4] J. Liang, Q. Yu, X. Yang, T. Zhang, and J. Li, Nano Res. **11**, 1599 (2018).
[5] B.-H. Lee, S. Park, M. Kim, A. K. Sinha, S. C. Lee, E. Jung, W. J. Chang, K.-S. Lee, J. H. Kim, S.-P. Cho, H. Kim, K. T. Nam, and T. Hyeon, Nat. Mater. **18**, 620 (2019).
[6] M.-M. Millet, G. Algara-Siller, S. Wrabetz, A. Mazheika, F. Girgsdies, D. Teschner, F. Seitz, A. Tarasov, S. V. Levchenko, R. Schlögl, and E. Frei, J. Am. Chem. Soc. **141**, 2451 (2019).
[7] S. Patnaik, D. P. Sahoo, and K. Parida, Renewable Sustainable Energy Rev. **82**, 1297 (2018).
[8] M. Makaremi, S. Grixti, K. T. Butler, G. A. Ozin, and C. V. Singh, ACS Appl. Mater. Interfaces **10**, 11143 (2018).
[9] J.-C. Liu, Y.-G. Wang, and J. Li, J. Am. Chem. Soc. **139**, 6190 (2017).
[10] K. Mao, L. Li, W. Zhang, Y. Pei, X. C. Zeng, X. Wu, and J. Yang, Sci. Rep. **4**, 5441 (2014).
[11] B. Qiao, J. Liu, Y.-G. Wang, Q. Lin, X. Liu, A. Wang, J. Li, T. Zhang, and J. Liu, ACS Catal. **5**, 6249 (2015).
[12] X.-K. Gu, B. Qiao, C.-Q. Huang, W.-C. Ding, K. Sun, E. Zhan, T. Zhang, J. Liu, and W.-X. Li, ACS Catal. **4**, 3886 (2014).
[13] Z. Chen, Q. Zhang, W. Chen, J. Dong, H. Yao, X. Zhang, X. Tong, D. Wang, Q. Peng, C. Chen, W. He, and Y. Li, Adv. Mater. **30**, 1704720 (2018).
[14] J. Zhang, J. Liu, L. Xi, Y. Yu, N. Chen, S. Sun, W. Wang, K. M. Lange, and B. Zhang, J. Am. Chem. Soc. **140**, 3876 (2018).
[15] I. X. Green, W. Tang, M. Neurock, and J. T. Yates, Science **333**, 736 (2011).
[16] Z.-Y. Li, Z. Yuan, X.-N. Li, Y.-X. Zhao, and S.-G. He, J. Am. Chem. Soc. **136**, 14307 (2014).
[17] J. Wan, W. Chen, C. Jia, L. Zheng, J. Dong, X. Zheng, Y. Wang, W. Yan, C. Chen, Q. Peng, D. Wang, and Y. Li, Adv. Mater. **30**, 1705369 (2018).
[18] R. Lin, D. Albani, E. Fako, S. K. Kaiser, O. V. Safonova, N. López, and J. Pérez-Ramírez, Angew. Chem. **131**, 514 (2019).
[19] S. Lee, C. Fan, T. Wu, and S. L. Anderson, J. Am. Chem. Soc. **126**, 5682 (2004).
[20] B. Yoon, H. Häkkinen, U. Landman, A. S. Wörz, J.-M. Antonietti, S. Abbet, K. Judai, and U. Heiz, Science **307**, 403 (2005).
[21] A. A. Herzing, C. J. Kiely, A. F. Carley, P. Landon, and G. J. Hutchings, Science **321**, 1331 (2008).
[22] G. J. Hutchings, M. S. Hall, A. F. Carley, P. Landon, B. E. Solsona, C. J. Kiely, A. Herzing, M. Makkee, J. A. Moulijn, A. Overweg, J. C. Fierro-Gonzalez, J. Guzman, and B. C. Gates, J. Catal. **242**, 71 (2006).
[23] M. F. Camellone and S. Fabris, J. Am. Chem. Soc. **131**, 10473 (2009).
[24] X. Zhou, Q. Shen, K. Yuan, W. Yang, Q. Chen, Z. Geng, J. Zhang, X. Shao, W. Chen, G. Xu, X. Yang, and K. Wu, J. Am. Chem. Soc. **140**, 554 (2018).
[25] Y.-G. Wang, D. C. Cantu, M.-S. Lee, J. Li, V.-A. Glezakou, and R. Rousseau, J. Am. Chem. Soc. **138**, 10467 (2016).
[26] M. H. Mahyuddin, Y. Shiota, and K. Yoshizawa, Catal. Sci. Technol. **9**, 1744 (2019).
[27] A. A. Mostofi, J. R. Yates, Y.-S. Lee, I. Souza, D. Vanderbilt, and N. Marzari, Comput. Phys. Commun. **178**, 685 (2008).
[28] N. Marzari, A. A. Mostofi, J. R. Yates, I. Souza, and D. Vanderbilt, Rev. Mod. Phys. **84**, 1419 (2012).
[29] J. Qiao, J. Zhou, Z. Yuan, and W. Zhao, Phys. Rev. B **98**, 214402 (2018).
[30] M. C. Romano, A. Vellasco-Gomes, and A. Bruno-Alfonso, J. Opt. Soc. Am. B **35**, 826 (2018).
[31] J. H. Ryoo, C.-H. Park, and I. Souza, Phys. Rev. B **99**, 235113 (2019).
[32] See Supplemental Material at http://link.aps.org/supplemental/10.1103/PhysRevLett.125.156001 for more details of methods and more results, which includes Refs. [27,33–48].
[33] G. Kresse and J. Furthmüller, Comput. Mater. Sci. **6**, 15 (1996).
[34] G. Kresse and J. Furthmüller, Phys. Rev. B **54**, 11169 (1996).
[35] J. P. Perdew, K. Burke, and M. Ernzerhof, Phys. Rev. Lett. **77**, 3865 (1996).
[36] P. E. Blöchl, Phys. Rev. B **50**, 17953 (1994).
[37] S. Grimme, J. Antony, S. Ehrlich, and H. Krieg, J. Chem. Phys. **132**, 154104 (2010).
[38] N. Marzari and D. Vanderbilt, Phys. Rev. B **56**, 12847 (1997).
[39] I. Souza, N. Marzari, and D. Vanderbilt, Phys. Rev. B **65**, 035109 (2001).
[40] J. Heyd, G. E. Scuseria, and M. Ernzerhof, J. Chem. Phys. **118**, 8207 (2003).
[41] G. Henkelman, B. P. Uberuaga, and H. Jónsson, J. Chem. Phys. **113**, 9901 (2000).
[42] S. A. Jafari, M. Jahanshahi, and M. Ghorbanzadeh Ahangari, Mater. Chem. Phys. **190**, 17 (2016).
[43] L. Zeng, C. Dai, B. Liu, and C. Xue, J. Mater. Chem. A **7**, 24217 (2019).
[44] P. Zhao, Y. Su, Y. Zhang, S.-J. Li, and G. Chen, Chem. Phys. Lett. **515**, 159 (2011).
[45] X. Zhang, J. Lei, D. Wu, X. Zhao, Y. Jing, and Z. Zhou, J. Mater. Chem. A **4**, 4871 (2016).
[46] X.-Y. Xu, J. Li, H. Xu, X. Xu, and C. Zhao, New J. Chem. **40**, 9361 (2016).

[47] X. Zhang, Z. Lu, and Z. Yang, J. Mol. Catal. A: Chem. **417**, 28 (2016).
[48] A. Kakekhani, L. T. Roling, A. R. Kulkarni, A. A. Latimer, H. Abroshan, J. Schumann, H. Aljama, S. Siahrostami, S. Ismailbeigi, F. Abildpedersen, and J. K. Nørskov, Inorg. Chem. **57**, **12**, 7222 (2018).
[49] S. Yang, W. Li, C. Ye, G. Wang, H. Tian, C. Zhu, P. He, G. Ding, X. Xie, Y. Liu, Y. Lifshitz, S.-T. Lee, Z. Kang, and M. Jiang, Adv. Mater. **29**, 1605625 (2017).
[50] L. Xie, L. Yang, W. Ge, X. Wang, and J. Jiang, Chem. Phys. **520**, 40 (2019).
[51] Y.-J. Yu, Y. Zhao, S. Ryu, L. E. Brus, K. S. Kim, and P. Kim, Nano Lett. **9**, 3430 (2009).
[52] M. Makaremi, B. Mortazavi, and C. V. Singh, J. Phys. Chem. C **121**, 18575 (2017).
[53] D. Stolcic, M. Fischer, G. Ganteför, Y. D. Kim, Q. Sun, and P. Jena, J. Am. Chem. Soc. **125**, 2848 (2003).
[54] L. D. Socaciu, J. Hagen, T. M. Bernhardt, L. Wöste, U. Heiz, H. Häkkinen, and U. Landman, J. Am. Chem. Soc. **125**, 10437 (2003).
[55] H. Tang, Y. Su, B. Zhang, A. F. Lee, M. A. Isaacs, K. Wilson, L. Li, Y. Ren, J. Huang, M. Haruta, B. Qiao, X. Liu, C. Jin, D. Su, J. Wang, and T. Zhang, Sci. Adv. **3**, e1700231 (2017).
[56] J.-H. Wang, M. Liu, and M. C. Lin, Solid State Ionics **177**, 939 (2006).
[57] Y. Xu, A. V. Ruban, and M. Mavrikakis, J. Am. Chem. Soc. **126**, 4717 (2004).
[58] N. Lopez and J. K. Nørskov, J. Am. Chem. Soc. **124**, 11262 (2002).
[59] B. Qiao, J.-X. Liang, A. Wang, C.-Q. Xu, J. Li, T. Zhang, and J. J. Liu, Nano Res. **8**, 2913 (2015).
[60] F. H. B. Lima, J. Zhang, M. H. Shao, K. Sasaki, M. B. Vukmirovic, E. A. Ticianelli, and R. R. Adzic, J. Phys. Chem. C **111**, 404 (2007).
[61] J. Zhang, H. Jin, M. B. Sullivan, F. C. H. Lim, and P. Wu, Phys. Chem. Chem. Phys. **11**, 1441 (2009).
[62] K. Ding, A. Gulec, A. M. Johnson, N. M. Schweitzer, G. D. Stucky, L. D. Marks, and P. C. Stair, Science **350**, 189 (2015).
[63] J. Mahmood, E. K. Lee, M. Jung, D. Shin, H.-J. Choi, J.-M. Seo, S.-M. Jung, D. Kim, F. Li, M. S. Lah, N. Park, H.-J. Shin, J. H. Oh, and J.-B. Baek, Proc. Natl. Acad. Sci. U.S.A. **113**, 7414 (2016).
[64] Z.-P. Liu, X.-Q. Gong, J. Kohanoff, C. Sanchez, and P. Hu, Phys. Rev. Lett. **91**, 266102 (2003).
[65] Y.-G. Wang, Y. Yoon, V.-A. Glezakou, J. Li, and R. Rousseau, J. Am. Chem. Soc. **135**, 10673 (2013).
[66] Z. Lu, P. Lv, Z. Yang, S. Li, D. Ma, and R. Wu, Phys. Chem. Chem. Phys. **19**, 16795 (2017).

Correction: A grant number contained an error and has been fixed.